# Short Papers

## Bragg Reflection Characteristics of Millimeter Waves in a Corrugated *H*-Guide

CHARRAY SURAWATPUNYA, MAKOTO TSUTSUMI, MEMBER, IEEE, AND NOBUAKI KUMAGAI, FELLOW, IEEE

*Abstract*—**The Bragg reflection characteristics of millimeter waves in a *H*-guide having a corrugated dielectric slab are investigated by the perturbation method of multiple scales. Brillouin diagrams in the vicinity of the Bragg frequency of the TM–TM-, TE–TE-, and TM–TE-mode couplings are shown. Validity of the theoretical predictions are confirmed by experiments carried out in the 40–50-GHz region. Typical frequency response at the stopband resulting from TM–TM-mode coupling is stop bandwidth about 380 MHz, with return loss about 2.1 dB at the Bragg frequency 47.3 GHz.**

### I. Introduction

Periodic structures in the form of periodic grooves in the surface of the dielectric structure have found widespread use in millimeter-wave integration applications such as band-reject filters [1], [2] and distributed Bragg reflector oscillators [3]. In such applications, the gratings would be operated in their stopbands, corresponding to Bragg reflection, in order to produce strong reflections.

Up to the present, a number of theoretical studies of waves in periodic structures have been presented in the literature. Among them a singular perturbation procedure which was proposed by Nayfeh [4], Asfar and Nayfeh [5], and Seshadri [6] is found to be an effective method. With the procedure, the authors have studied the electromagnetic wave interactions in a surface-corrugated dielectric slab [2] and shown that the numerical results agree well with experimental data.

In this short paper, the electromagnetic wave interactions in a *H*-guide [7], [8] having a surface-corrugated dielectric slab are studied. The method of analysis based on the perturbation method of multiple scales [4]–[6] is employed. The dispersion characteristics around the Bragg interaction region of the TM–TM-, TE–TE-, and TM–TE-mode couplings as a function of slab width are determined and compared with the experimental data performed in the 40–50-GHz range.

### II. Theoretical Consideration

Geometry of a corrugated *H*-guide is shown in Fig. 1 [7], [8]. The dielectric slab occupying the regions $-b/2 < y < b/2$ and $-a/2 < z < z(x)$ between two parallel metal plates has the top boundary surface $z = z(x)$ that varies sinusoidally in the $x$ direction. If the surface undulation is assumed to be small with parameter $\delta$, the boundary surface along $z(x)$ can be defined as

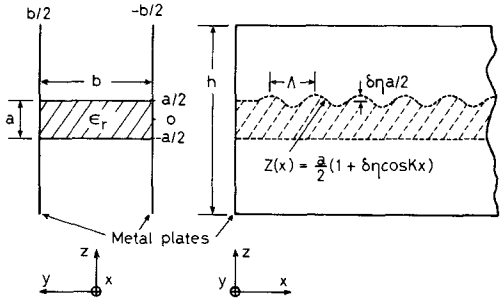


Fig 1 Geometry of a corrugated *H*-guide and the system of coordinates for the analysis.

$$z(x) = \frac{a}{2}(1 + \delta\eta\cos Kx) \tag{1}$$

where $\eta$ and $2\pi/K = \Lambda$ are the modulation index and the spatial periodicity of the undulation, respectively. We shall consider only guided waves that propagate in the $x$ direction and having the time dependence $\exp(j\omega t)$, where $\omega$ is the wave angular frequency.

There are two types of hybrid modes, classified as the $TM^z_{pq}$ and $TE^z_{pq}$ modes where the subscripts $p$ and $q$ indicate the number of extrema of the field in the $y$ and $z$ directions, respectively, that the *H*-guide can support [8]. Fig. 2(a) shows the dispersion diagrams of the lowest order of these modes for the case of slab thickness $a = 3.16$ mm, width $b = 3.80$ mm, and relative dielectric constant $\epsilon_r = 2.0$. Without periodic corrugations on a surface of the slab, the forward ($n = 0$) and backward ($n = -1$) $TM^z$ and $TE^z$ modes propagate independently along the guide. When weak sinusoidal corrugations are presented, an incident $TM^z$ (or $TE^z$) wave will not only produce a transmitted and a reflected $TM^z$ (or $TE^z$) wave but also excite a transmitted and a reflected $TE^z$ (or $TM^z$) wave. As a consequence of these mode conversion effects the first-order coupling of $TM^z$–$TM^z$, $TE^z$–$TE^z$, and $TM^z$–$TE^z$ modes will take place at the intersection points $A$, $B$ and $C$, $D$, respectively. Such mode conversion effects have recently been observed in the periodically-corrugated dielectric waveguide of finite width such as rectangular dielectric image guide [9]. To study the characteristics of wave interactions in the vicinity of the interaction points $A$ to $D$, analysis by the perturbation method of multiple scales is employed.

In terms of scalar potentials $\phi^h$ and $\phi^e$ which define the $TM^z$ and $TE^z$ modes, it is possible to write electric field and magnetic field as follows [10]:

$$\mathbb{E} = \omega^2\mu_0\epsilon_0\epsilon_r\hat{z}\phi^h + \nabla(\nabla\cdot\hat{z}\phi^h) - j\omega\mu_0\nabla\times\hat{z}\phi^e$$
$$\mathbb{H} = j\omega\epsilon_0\epsilon_r\nabla\times\hat{z}\phi^h + \omega^2\mu_0\epsilon_0\epsilon_r\hat{z}\phi^e + \nabla(\nabla\cdot\hat{z}\phi^e). \tag{2}$$

Manuscript received July 13, 1982; revised February 25, 1983.

The authors are with the Department of Electrical Communication Engineering, Osaka University, Yamada Oka, Suita, Osaka 565, Japan.

0018-9480/83/0700-0584$01.00 ©1983 IEEE

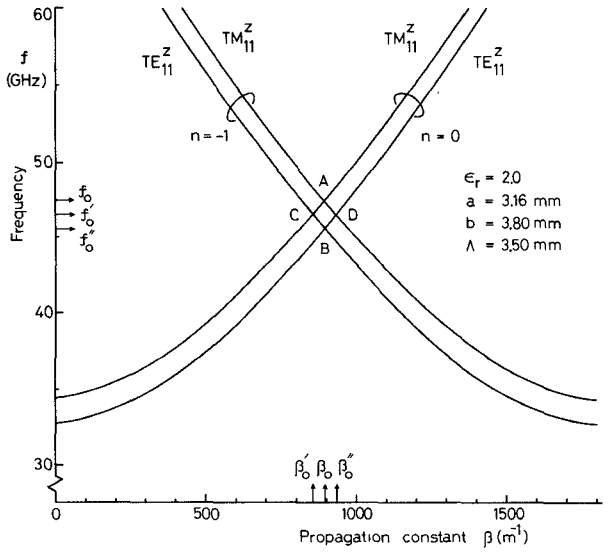


(a)

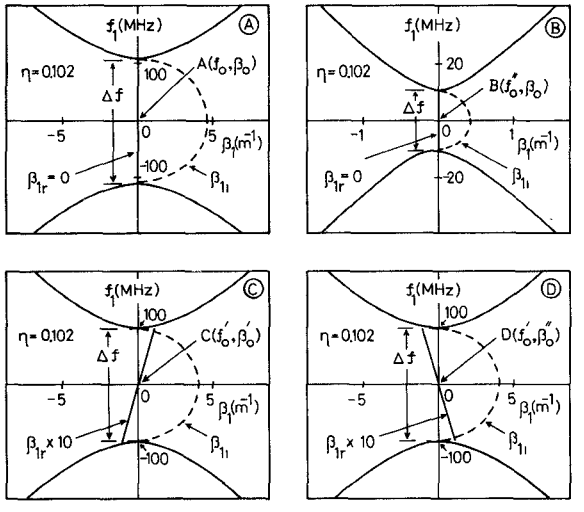


(b)

Fig. 2. (a) Zeroth-order dispersion diagrams for slab thickness $a = 3.16$ mm and width $b = 3.80$ mm. (b) The first-order stopband characteristics in the vicinity of the interaction points $A$, $B$, $C$, and $D$ for the index of undulation $\eta = 0.102$. The solid curve is the real part and the dashed curve is the imaginary part of wavenumber $\beta_1$.

The scalar potentials $\phi^h$ and $\phi^e$ satisfy the wave equation

$$\nabla^2\phi^i + \omega^2\mu_0\epsilon_0\epsilon_r\phi^i = 0, \qquad i = h, e. \tag{3}$$

In the above expressions $\nabla = \hat{x}\partial/\partial x + \hat{y}\partial/\partial y + \hat{z}\partial/\partial z$ and $\epsilon_r$ is the relative dielectric constant of the slab. Following the singular perturbation procedure using the method of multiple scales [4]–[6], we introduce an expansion of $\omega$ around Bragg frequency $\omega_0$ as

$$\omega = \omega_0 + \delta\omega_1. \tag{4}$$

Perturbation expansions of the wave potentials $\phi^i$ and the fields $\mathbb{E}$ and $\mathbb{H}$ in a series of $\delta$ are carried out in the form

$$F(x, y, z) = F_0(x_0, x_1, y, z) + \delta F_1(x_0, x_1, y, z) \tag{5}$$

where $F_0$ represents the unperturbed zeroth-order quantities $\phi_0^i$, $\mathbb{E}_0$, and $\mathbb{H}_0$, and $F_1$ represents the perturbed first-order quantities $\phi_1^i$, $\mathbb{E}_1$, and $\mathbb{H}_1$. The chain rule of differentiation with respect to $x$ yields

$$\frac{\partial}{\partial x} = \frac{\partial}{\partial x_0} + \delta\frac{\partial}{\partial x_1}. \tag{6}$$

At the air–dielectric interfaces of $z = z(x)$ and $z = -a/2$, the required boundary conditions are obtained from the continuity of tangential components of the electric and magnetic field as

$$E_x + \frac{dz(x)}{dx}E_z = E_x^0 + \frac{dz(x)}{dx}E_z^0, \quad H_y = H_y^0 \tag{7}$$

$$H_x + \frac{dz(x)}{dx}H_z = H_x^0 + \frac{dz(x)}{dx}H_z^0, \quad E_y = E_y^0, \qquad z = z(x) \tag{8}$$

and

$$E_x = E_x^0, \quad H_y = H_y^0 \tag{9}$$

$$H_x = H_x^0, \quad E_y = E_y^0, \qquad z = -a/2 \tag{10}$$

where $dz(x)/dx$ is the gradient of the surface corrugation which can be determined from (1), and the superscript zero on the fields denotes the fields in the air region. To determine the boundary conditions for the zeroth-order and the first-order of $\delta$, we first expand the tangential components of the electric and magnetic field in (7)–(10) with the help of (2), (4), (5), and (6) and then carry out Taylor series expansions around $z = a/2$ up to linear term in $\delta$ of the fields in (7) and (8). After equating the coefficients of equal powers of $\delta$, the zeroth-order and the first-order boundary conditions in terms of $\phi_0^i$ and $\phi_1^i$ along $z = \pm a/2$ can be obtained.

The derivation of the coupled-mode equations that govern the nature of the first-order Bragg interaction of TM$^z$–TM$^z$ waves will be performed first. Since the TE$^z$ modes are nonresonant with the forward and backward TM$^z$ modes at the interaction point $A$, we shall take the zeroth-order fields belonging to the TE$^z$ modes ($\phi_0^e$) equal to zero. Substituting (4)–(6) into (3) and equating the coefficients of equal powers of $\delta$, the zeroth- and first-order differential equations for $\phi_0^h$, $\phi_1^h$, and $\phi_1^e$ can be obtained. Substituting the solutions of the zeroth-order differential equation satisfied by $\phi_0^h$ into the zeroth-order boundary conditions calculated from (7)–(10), the zeroth-order dispersion relation describing the dispersion curves of the TM$^z$ mode in Fig. 2(a) is obtained [7], [8]

$$\tan(k_h a/2) = \epsilon_r\alpha_h/k_h \tag{11}$$

where

$$\alpha_h = \sqrt{\beta_h^2 + k_y^2 - \omega_0^2\mu_0\epsilon_0}, \quad k_h = \sqrt{\omega_0^2\mu_0\epsilon_0\epsilon_r - \beta_h^2 - k_y^2}$$

and

$$k_y = p\pi/b, \qquad p = 1 \text{ for the fundamental mode.}$$

The forward and backward TM$^z$ modes couple to each other at the intersection point $A$ where the Bragg condition or resonant condition

$$\beta_h = K/2 = \pi/\Lambda \tag{12}$$

is satisfied. The value of frequency corresponding to the intersection point is the Bragg frequency. For the zeroth-order unperturbation problem, it is seen that TM$^z$-mode fields alone satisfy the zeroth-order boundary conditions. But for the first-order boundary perturbation problem, it should be noted that a superposition of the TM$^z$- and TE$^z$-mode fields is required for the satisfaction of the first-order boundary conditions. This is because the perturbations in the boundary surface of the slab also produce modes of TE$^z$ wave when the waveguide excitation is only TM$^z$; however, these TE$^z$ modes are of order of $\delta$ and do not resonate with the TM$^z$ mode at the interaction point $A$. As a result of this nonresonant coupling, the first-order fields of the TE$^z$ modes ($\phi_1^e$) must be taken into account.

When solutions of $\phi_0^h$ and $\phi_0^e (= 0)$ are known, the solutions for $\phi_1^h$ and $\phi_1^e$ can be obtained from the first-order differential

equations. Substituting $\phi_0^h$, $\phi_1^h$, and $\phi_1^e$ into the first-order boundary conditions calculated from (7)–(10), and using orthogonality of Floquet modes, the coupled-mode equations governing the nature of the interaction between the forward and backward lowest order TM$^z$ modes can be deduced as

$$\left(\omega_1 - jv_g^+ \frac{\partial}{\partial x_1}\right) A_0^+ = \eta c^{+-} A_0^-$$

$$\left(\omega_1 + jv_g^- \frac{\partial}{\partial x_1}\right) A_0^- = \eta c^{-+} A_0^+ \tag{13}$$

where

$$v_g^+ = v_g^- = v_g^h = \frac{\beta_h\left[\frac{a}{2}\alpha_h\left(k_h^2+\epsilon_r^2\alpha_h^2\right)+\epsilon_r\left(k_h^2+\alpha_h^2\right)\right]}{\omega_0\mu_0\epsilon_0\epsilon_r\left[\frac{a}{2}\alpha_h\left(k_h^2+\epsilon_r^2\alpha_h^2\right)+\left(\epsilon_r\alpha_h^2+k_h^2\right)\right]}$$

is the group velocity, and $c^{+-}$, $c^{-+}$ are the coupling coefficients given by

$$c^{+-} = c^{-+} = c^h = -\frac{1}{4}\frac{a}{2}\frac{\alpha_h k_h^2\left[\beta_h^2\left(k_h^2-\epsilon_r^2\alpha_h^2+2\epsilon_r\alpha_h^2\right)+k_y^2\left(k_h^2+\epsilon_r^2\alpha_h^2\right)\right]}{\omega_0\mu_0\epsilon_0\epsilon_r\left(\beta_h^2+k_y^2\right)\left[\frac{a}{2}\alpha_h\left(k_h^2+\epsilon_r^2\alpha_h^2\right)+\left(\epsilon_r\alpha_h^2+k_h^2\right)\right]}.$$

$A_0^+$ and $A_0^-$ are the amplitudes of the forward and backward TM$^z$ modes, respectively. The coupled-mode equations that govern the nature of the first-order Bragg interaction of the TE$^z$–TE$^z$ modes and the TM$^z$–TE$^z$ modes can be derived in the same manner and only the results are listed below. The form of coupled-mode equations are given by (13) but with the following conditions.

a) For TE$^z$–TE$^z$ coupling (at point $B$)

$$v_g^+ = v_g^- = v_g^e = \frac{\beta_e\left[\left(k_e^2+\alpha_e^2\right)\left(\frac{a}{2}\alpha_e+1\right)\right]}{\omega_0\mu_0\epsilon_0\left[\frac{a}{2}\epsilon_r\alpha_e\left(k_e^2+\alpha_e^2\right)+\left(\epsilon_r\alpha_e^2+k_e^2\right)\right]}$$

and

$$c^{+-} = c^{-+} = c^e = \frac{1}{4}\frac{a}{2}\frac{\alpha_e k_e^2\left(k_e^2+\alpha_e^2\right)\left(\beta_e^2-k_y^2\right)}{\omega_0\mu_0\epsilon_0\left(\beta_e^2+k_y^2\right)\left[\frac{a}{2}\epsilon_r\alpha_e\left(k_e^2+\alpha_e^2\right)+\left(\epsilon_r\alpha_e^2+k_e^2\right)\right]}. \tag{14}$$

$A_0^+$ and $A_0^-$ represent the forward and backward TE$^z$-wave amplitudes, respectively. The wavenumber $\beta_e$ satisfies the zeroth-order dispersion relation for TE$^z$ mode [8]

$$\tan\left(k_e a/2\right) = \alpha_e/k_e.$$

b) For TM$^z$–TE$^z$ coupling (at point $C$)

$$v_g^+ = v_g^h, \quad v_g^- = v_g^e$$

$$c^{+-} = c^{he} = \frac{1}{4}\frac{a}{2}k_y\frac{\left(\cos k_e\frac{a}{2}\right)\left(\alpha_h k_h\right)^2\left(k_e^2+\alpha_e^2\right)\left(\beta_h+\beta_e\right)}{\omega_0^2\mu_0\epsilon_0^2\epsilon_r\left(\cos k_h\frac{a}{2}\right)\left(\beta_h^2+k_y^2\right)\cdot\left[\frac{a}{2}\alpha_h\left(k_h^2+\epsilon_r^2\alpha_h^2\right)+\left(\epsilon_r\alpha_h^2+k_h^2\right)\right]}$$

and

$$c^{-+} = c^{eh} = \frac{1}{4}\frac{a}{2}k_y\frac{\left(\sin k_h\frac{a}{2}\right)\alpha_e k_e^2 k_h\left(\epsilon_r-1\right)\left(\beta_h+\beta_e\right)}{\mu_0\left(\cos k_e\frac{a}{2}\right)\left(\beta_e^2+k_y^2\right)\cdot\left[\frac{a}{2}\epsilon_r\alpha_e\left(k_e^2+\alpha_e^2\right)+\left(\epsilon_r\alpha_e^2+k_e^2\right)\right]}. \tag{15}$$

$A_0^+$ and $A_0^-$ represent the amplitudes of the forward TM$^z$ and the backward TE$^z$ wave, respectively.

c) For TM$^z$–TE$^z$ coupling (at point $D$)

$$v_g^+ = v_g^e, \quad v_g^- = v_g^h$$

$$c^{+-} = -c^{eh} \quad \text{and} \quad c^{-+} = -c^{he}. \tag{16}$$

$A_0^+$ and $A_0^-$ represent the amplitudes of the forward TE$^z$ and the backward TM$^z$ wave, respectively.

For a special case when the slab width is extended to infinity on both sides, i.e., $b \to \infty$, it is interesting to note that (13) with $k_y \to 0$ correctly reduce to the same coupled-mode equations of the TM wave as given in [2]. Also, when $k_y \to 0$, (15) and (16) show that $c^{he} = c^{eh} = 0$, and that the TM$^z$–TE$^z$ coupling appears only for finite slab width, which agrees with that discussed by Shiau *et al.* [9].

If the amplitude $A_0^+$ has the form of $A_0^+ = A_{00}^+ \exp(-j\beta_1 x_1)$ where $A_{00}^+$ is a constant, the first-order dispersion relation can be deduced from the coupled-mode equations. Estimating numerically the first-order dispersion relation for TM$^z$–TM$^z$, TE$^z$–TE$^z$, and TM$^z$–TE$^z$ couplings, the Brillouin diagrams near the interaction points $A$, $B$, $C$, and $D$ are shown in Fig. 2(b). The numerical value of parameters are given in the figure, and $\beta_1$ and $f_1$ are, respectively, the perturbed propagation constant and frequency from the unperturbed values $(\beta_0, f_0)$ at the intersection point. From Fig. 2(b) it is seen that, within the stopband region, the real part of the wavenumber in the case of TM$^z$–TE$^z$ coupling varies linearly with frequency, while in the case of TM$^z$–TM$^z$ or TE$^z$–TE$^z$ coupling it remains a constant at its zeroth-order value. The variation of the Bragg frequency $f_0$ and the stop bandwidth $\Delta f$ on the slab width for three types of couplings are plotted in Fig. 3. It is seen that the Bragg frequency of the three different couplings decreases with increasing the slab width. The stop bandwidth of the TM$^z$–TM$^z$ and the TM$^z$–TE$^z$ couplings also decreases as the slab width increases. But the stop bandwidth of the TE$^z$–TE$^z$ coupling increases with the slab width after it vanishes once at $b = 3.50$ mm. The vanishing value of the stop bandwidth at $b = 3.50$ mm shows that there exists the Brewster phenomenon in the TE$^z$–TE$^z$ coupling. From Fig. 3 it is noted that the stop bandwidth due to TM$^z$–TE$^z$ coupling is slightly narrower than that of the TM$^z$–TM$^z$ coupling.

In practice, the periodic structure is restricted within a finite length, assuming from $x = 0$ to $x = L$ in the direction of wave propagation. Solving the coupled-mode equations (13) subject to the phenomenological boundary condition that backward wave amplitude $A_0^-(x = L) = 0$, the complex reflection coefficient $R$ can be deduced [6]. Fig. 4 shows the value of $R$ resulting from TM$^z$–TM$^z$-mode coupling as a function of frequency in the vicinity of the Bragg frequency for the number of elements in the surface corrugation $N = 70$. For $\epsilon_r = 2.0$, $a = 3.16$ mm, $b = 3.80$ mm, and $\eta = 0.102$, it can be estimated from Fig. 4 that the half-power bandwidth is about 385 MHz and return loss is about 1.81 dB. Only the reflection coefficient for TM$^z$–TM$^z$-mode coupling is considered because this case is available for the experiment described later.

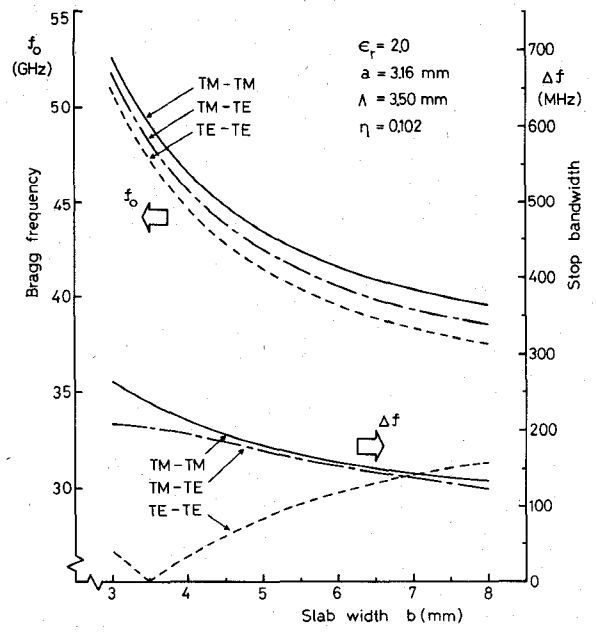


Fig. 3. Variation of Bragg frequency and stop bandwidth obtained from the Brillouin diagram as a function of slab width for $TM_{11}^z$–$TM_{11}^z$-, $TM_{11}^z$–$TE_{11}^z$-, and $TE_{11}^z$–$TE_{11}^z$-mode couplings.

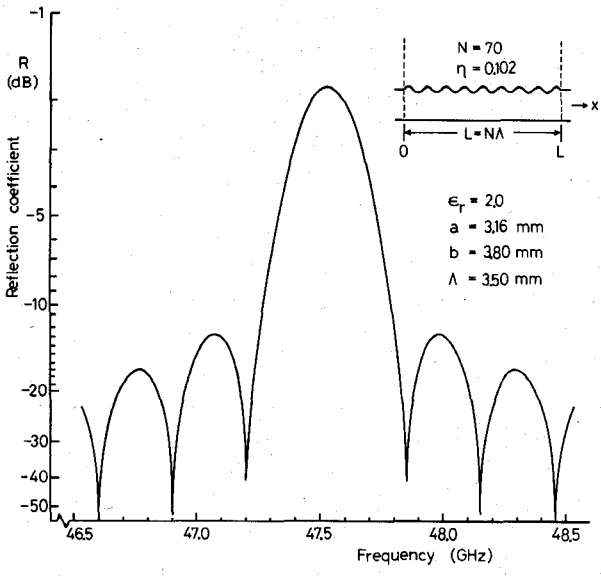


Fig. 4. Computed reflection coefficient for $TM_{11}^z$–$TM_{11}^z$-mode coupling.

## III. Experimental Results and Discussions

In order to demonstrate the validity of the theoretical predictions described in the previous section, experiments on the reflection characteristics have been performed in the millimeter-wave region. The *H*-guide tested consists of two parallel $10 \times 26$ cm$^2$ copper plates and a Teflon slab with relative dielectric constant $\epsilon_r = 2.0$. Dimensions of the slab are thickness 3.16 mm, width 3.80 mm, and length 340 mm. One surface of the slab is corrugated with rectangular grooves by milling machine to form a periodic surface undulation in the propagation direction. The width, depth, and periodicity of the groove and the number of corrugations are 1.50 mm, 0.26 mm, 3.50 mm, and $N = 70$, respectively. When estimating from the Fourier series expansion of the shape of the corrugations, the value of the modulation index $\eta$ used in the computation is found to be 0.102.

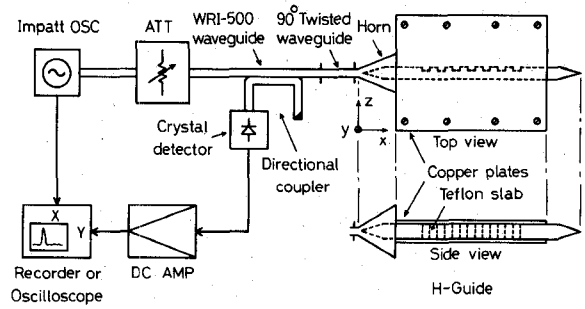


Fig. 5. Bragg reflection measurement setup.

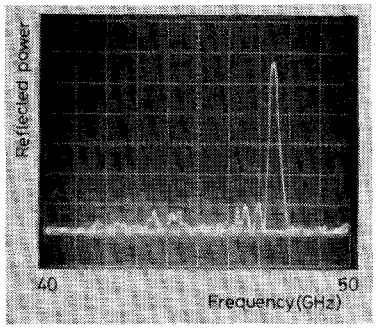


Fig. 6. Typical measured reflection characteristics of the millimeter wave from a corrugated *H*-guide when $TM_{11}^z$ mode is excited.

The experimental setup is shown in Fig. 5. The millimeter-wave power sweeping in the frequency range 40–50 GHz is fed to the *H*-guide through an electromagnetic horn antenna. Since the principal field components of the $TM^z$ mode are $E_z$ and $H_y$, the guide is set in the position that the copper plates plane is in parallel to the *E*-plane of the horn antenna, which is in turn coupled directly to the WRI-500 waveguide ($TE_{10}$ mode) to excite the $TM^z$ mode. The slab has tapered transition sections at the front end which is inserted into the horn antenna to gradually shape the field pattern of the $TE_{10}$ mode at the rectangular waveguide end to the field of the $TM_{11}^z$ mode at the *H*-guide end, and also at the far end to avoid unwanted reflection. Bragg reflections caused by the interaction of the lowest mode of $TM^z$ wave are detected through a directional coupler and are recorded by *X*–*Y* recorder or oscilloscope. Fig. 6 shows the photograph of the typical measured reflection characteristics from the corrugated *H*-guide at stopband. The bandwidth of the stopband as measured is about 380 MHz, with return loss about 2.1 dB at the Bragg frequency 47.3 GHz. Since the waves in the corrugated *H*-guide are excited and detected through the rectangular waveguide which operates in the $TE_{10}$ mode where the amplitude of the transverse electric field ($E_z$) is maximum at the center of the waveguide, it should be noted that only the $TM_{11}^z$ mode in the *H*-guide, which has similar field distribution and polarization to the $TE_{10}$ mode, can be excited and detected. The $TE_{11}^z$ mode having $E_z = 0$ and zero transverse electric field ($E_y$) at the center of the guide then cannot be excited or detected through rectangular waveguide. Due to the difference in polarization and transverse field distribution mentioned above, measurements on the Bragg reflection due to $TM_{11}^z$–$TE_{11}^z$-mode coupling when $TM_{11}^z$ mode is excited as well as $TE_{11}^z$–$TE_{11}^z$-mode coupling are unavailable in the present experimental setup shown in Fig. 5. A method for measurement of a reflected signal caused by TM–TE-mode coupling when only TM mode is excited in a corrugated *H*-guide, by opening a thin slit in the metal plate perpendicular to direction of propagation and measuring a reflected signal associated

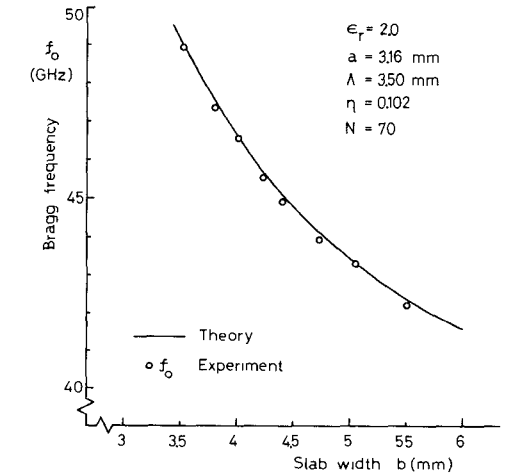


(a)

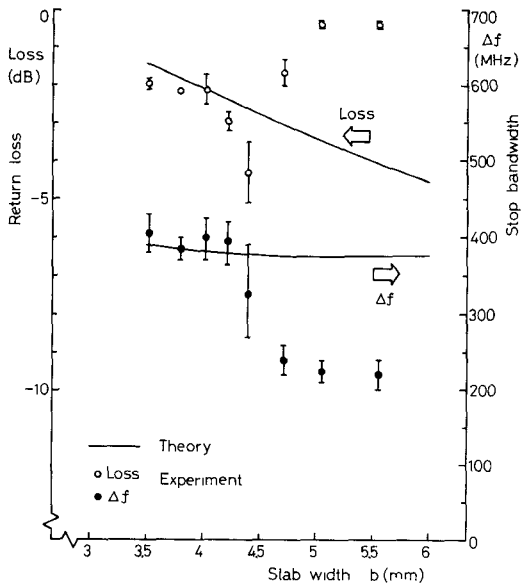


(b)

Fig. 7. Comparison between experiment and theory obtained from the reflection coefficient for $TM_{11}^z$–$TM_{11}^z$-mode coupling as a function of slab width for $N = 70$. (a) Bragg frequency. (b) Return loss and half-power bandwidth.

with the TE mode at the slit by a probe, has been reported in [11].

To make qualitative comparison of the theory with experiments, we have repeated the experiments on the Bragg reflection of $TM_{11}^z$ mode from corrugated $H$-guide for several slab widths between 3.52 mm and 5.55 mm, while the other dimensions are kept constant. In the experiment, the copper plates are kept parallel at the given spacing equal to the slab width by the screws. Since it is very difficult to adjust the screws to keep the space between the plates accurately equal throughout the length of the guide, the measured stopband responses are slightly affected. Fig. 7(a) and (b) shows the plots of Bragg frequency $f_0$ and the return loss and half-power bandwidth $\Delta f$ as a function of slab width of the measured and computed results. The computed results shown by the solid curves are obtained from the reflection coefficient of Fig. 4. From these figures it is seen that the measured Bragg frequencies agree well with the computed ones. The agreement of both return loss and half-power bandwidth is also good for narrow slab width (smaller than $b = 4.40$ mm). As the slab width increases, the difference between the measured and the predicted data is evident. The measured return losses are higher while the measured half-power bandwidths are lower than the computed results. These discrepancies seem to arise mainly from the use of phenomenological boundary conditions described in the preceding section. This is so because the reflection coefficient for the finite periodic structure is derived under the assumption that the variation of the fields in the transverse ($y$ and $z$) direction are the same for both outside and inside the grating region, and the fields are matched only at the center portion of the slab (one-dimensional boundary value problem [2], [6]). The theory is limited to be accurate for narrow slab width. Another source of discrepancies seems to arise from the mismatching effects at the transition section between the rectangular waveguide and the tested waveguide. Since the dimensions of the rectangular waveguide and horn antenna are unchanged, widening the slab width should cause additional reflected power from the tapered section of the tested waveguide.

## IV. Conclusions

The electromagnetic wave interactions in a corrugated $H$-guide have been investigated theoretically and experimentally. By a singular perturbation procedure, the dispersion and the reflection characteristics in the vicinity of the Bragg frequency of the TM–TM-, TE–TE-, and TM–TE-mode couplings were derived. Numerical results for the reflection coefficients caused by TM–TM-mode coupling for several slab widths have been compared with the experiments in the millimeter-wave frequency. The agreement was found to be good only for narrow dielectric slab widths. The sources of discrepancies between theory and experiment for wide slab widths were briefly discussed.

The low-loss properties and the simple structure of the corrugated $H$-guide may be useful for applications in millimeter-wave integrated circuits as a band-reject filter, as well as in a high $Q$ (over 200) resonator if a large slab width or double-corrugated dielectric slab is used.

## References

[1] T Itoh, "Application of gratings in a dielectric waveguide for leaky-wave antennas and band-reject filters," *IEEE Trans. Microwave Theory Tech.*, vol. MTT-25, pp. 1134–1138, Dec. 1977.

[2] M. Tsutsumi, T. Ohira, T. Yamaguchi, and N. Kumagai, "Reflection of millimeter waves by a corrugated dielectric slab waveguide," *Proc. IEEE*, vol-68, pp. 733–734, June 1980.

[3] T Itoh and F Hsu, "Distributed Bragg reflector Gunn oscillators for dielectric millimeter-wave integrated circuits," *IEEE Trans. Microwave Theory Tech.*, vol. MTT-27, pp. 514–518, May 1979.

[4] A. H. Nayfeh, *Introduction to Perturbation Techniques*. New York: Wiley-Interscience, 1981.

[5] O. R. Asfar and A. H. Nayfeh, "Stopbands of the first-order Bragg interaction in a parallel-plate waveguide having multiperiodic wall corrugations," *IEEE Trans. Microwave Theory Tech.*, vol. MTT-28, pp. 1187–1191, Nov. 1980.

[6] S. R. Seshadri, "Reflection by a sinusoidally modulated surface reactance at oblique incidence," *IEEE Trans Microwave Theory Tech.*, vol. MTT-29, pp. 594–600, June 1981.

[7] F. J. Tischer, "Properties of the $H$-guide at microwave and millimeter-wave regions," *Proc. IEE*, vol. 106B, pp. 47–53, Jan. 1959.

[8] J. W. E. Griemsmann and L. Birenbaum, "A low-loss $H$-guide for millimeter wavelengths," in *Proc. Symp. Millimeter Waves*, 1959, pp. 543–562.

[9] M. J. Shiau, H. Shigesawa, S. T. Peng, and A A. Ohner, "Mode conversion effects in Bragg reflection from periodic grooves in rectangular dielectric image guide," in *IEEE 1981 MTT Symp. Dig.*, June 15–19, 1981, pp. 14–16.

[10] R. F Harrington, *Time-Harmonic Electromagnetic Fields*. New York: McGraw-Hill, 1961, pp. 129–132.

[11] S. Matsumoto, M. Tsuji, H. Shigesawa, and K. Takiyama, "On the experimental investigations of finite periodic corrugation in open dielectric waveguides," Inst. Electronics Communications Eng. Japan, Apr. 1982, Tech. Group Pap. MW82-2, pp. 9–15.